Increase of the energy available for snow ablation in the Pyrenees (1959–2020) and its relation to atmospheric circulation

Josep Bonsoms [a,*], Juan Ignacio López-Moreno [b], Sergi González [c], Marc Oliva [a]

[a] Department of Geography, Universitat de Barcelona, Barcelona, Catalonia, Spain
[b] Instituto Pirenaico de Ecología (IPE-CSIC), Campus de Aula Dei, Zaragoza, Spain
[c] Antarctic Group, Spanish Meteorological Agency (AEMET), Barcelona, Catalonia, Spain

ABSTRACT

Mid-latitude mountain snowpacks are highly vulnerable to climate warming. Past and future hydroclimate changes require a thourogout knowledge of snow ablation physical processes and the associate climate drivers. In this work we provide the first spatio-temporal characteritzation of the energy available for snow ablation (Q_m) in the Pyrenees for the period 1959–2020, during the main ablation season (March to June) for low (1200 m), mid (1800 m) and high (2400 m) elevations. We analyze the role of the the main Circulation Weather Types (CTs) in the Q_m components for the entire mountain range. Finally, we train and tune a machine learning algorithm, the Random Forest, with atmospheric data (Surface Level Pressure and 500 hPa Geopotential Height) as an independent variable and Q_m as the dependent one, in order to determine how much of the observed changes in Q_m can be related with atmospheric circulation variability. The largest contribution of Q_m is Net Radiation (Rn), increasing with elevation. Q_m has shown a statistically significant increase since the 1980s. The comparison between the period 1959–1980 and the 2000–2020 revealed that positive Q_m fluxes have been anticipated 22 and 12 days at mid and high elevations, respectively, showing evidence of an advance in the timing of the ablation season and faster snow ablation in high-elevation areas of the Pyrenees. The Q_m is principally driven by Rn during the prevailing antyciclonic situations, characterized by the extension of high-pressure systems, low-barometric gradients and the SE advection of hot and dry air masses. The positive frequency of these anticyclonic CTs explains the majority (75%) of the Qm variability, the upward Qm trends and the earlier snow ablation onset since the 1980s.

1. Introduction

Mid-latitude mountain ranges have been exposed to major environmental changes over the last decades (Hock et al., 2019). In the Pyrenees, the climate warming recorded since the end of the Little Ice Age (ca. 1850 CE) has critically affected the cryosphere (Oliva et al., 2018). The remaining glaciers in this mountain range have undergone a significant recession in recent years and are expected to disappear by the mid of the 21st century (López-Moreno et al., 2016; Rico et al., 2017; Vidaller et al., 2021). In addition, a negative trend in snow depth (HS) and duration was found for the entire range from 1958 to 2017 (López-Moreno et al., 2020a, 2020b). Changes in the snow regime and timing have significant impacts on mountain ecosystems; including, but not limited to, modifications of the geoecological, hydrological (e.g., García-Ruiz et al., 2011) and biological cycles (e.g., Vorkauf et al., 2021). Snow

scarcity has also major socioeconomic implications, such as determining a decrease of the hydropower production (e.g., Gascoin et al., 2015) or a shortening of the snow tourism season (Gilaberte-Búrdalo et al., 2017), among others.

Climate projections anticipate significant warming over mid-latitude mountain ranges in the forthcoming decades (IPCC, 2021), with higher temperature increases in Mediterranean mountains than in other mid-latitude ranges (Nogués-Bravo et al., 2008). In the Pyrenees, high emission climate scenarios, project an increase of the intensity and frequency (ca. + 20%) of high snowfall events at high elevation areas (> 2500 m), although a significant reduction of the intensity (− 60%) and frequency (− 80%) is expected to occur between 1000 and 1500 m (López-Moreno et al., 2011). The duration of the snow season is expected to decrease by ca. 20–30 days per °C (López-Moreno et al., 2013). Under a climate warming of >2 °C the snow season would reduce by ca.

38% (15%) in the lowest (highest) elevation areas with south (north) orientation of the eastern (western) Pyrenees (Pons et al., 2015).

The projected climate changes require a better understanding of the hydro-climatological patterns prevailing nowadays in the Pyrenees. In this sense, identifying to which extent the observed changes in snow-pack magnitude and timing are mostly related to a decline in snow accumulation or to an increase in the melt rates or a combination of both, would help to better anticipate the consequences of climate projections for the snowpack and the spatio-temporal dynamics of hydrological processes in the headwaters of the valleys. In this study, we focus on the melting period, and aim to quantify changes in the snow Surface Energy Balance (SEB) that could be driving changes in the amount of energy available for snow ablation (Q_m). From a climatological perspective, it remains unknown whether the Q_m evolution over the past 60 years has been mainly driven by anomalies on the prevailing Circulation Weather types (CTs) or by superimposed long-term climate trends that could be associated to anthropogenic climate change. In recent years, several studies have analyzed the influence of the CTs on the snowfall in the high lands of the central (Esteban et al., 2005), western and central Pyrenees (López-Moreno and Serrano-Vicente, 2006; Navarro-Serrano and López-Moreno, 2017). Changes in the frequency of the CTs have been associated with the snow trends at low-mid elevations (Buisán et al., 2014) as well as at high elevations of this mountain range (Bonsoms et al., 2021a). To date, only a few studies in other regions have explored the links between the CTs and the snowpack Q_m components, such as in the Great Plains (Grundstein and Leathers, 1999) and the Great Lakes of North America (Suriano and Leathers, 2018), in the Tokachi region of Japan (Hayashi et al., 2005) or in the Australian Alps (Schwartz et al., 2020). However, the Q_m energy portioning is still unknown in the Pyrenees. The objective of this paper is to shed light on these issues responding the following questions:

(i) What changes occurred on the Q_m during the snow ablation phase (March to June) between 1959 and 2020 by elevation and geographical areas of the Pyrenees?

(ii) Which was the impact of the CTs on the Q_m by elevation and sectors of the Pyrenees?

(iii) How much Q_m can be related with atmospheric circulation changes, instead of other physical processes?

For the first objective, we analyzed the contribution of the Q_m components together with the spatiotemporal evolution of the Q_m trends at low (1200 m), mid (1800 m) and high (2400 m) specific elevation ranges of the Pyrenees. In order to provide a better characterization of the climate drivers of the snow ablation events, we performed a CT classification and quantified the impact of each synoptic situation on the Q_m. Finally, we quantified how much of the average seasonal Q_m can be linked to changes in atmospheric circulation rather than other physical processes (i.e., land-atmosphere feedbacks) by means of a Random Forest (RF) regression modeled with atmospheric data.

2. Geographical and climatic setting

The Pyrenees is a long (ca. 450 km) mountain range located in Southern Europe (42°N-43°N to 2°W-3°E) that extends between the Atlantic Ocean (W) and the Mediterranean Sea (E). The elevation increases towards the center of the mountain range, where the highest peaks are found (Aneto, 3404 m asl), and decreases towards the edges. The climate of the Pyrenees is ruled by the southward displacement of the jet stream during winter, and anticyclonic conditions during summer (Bonsoms et al., 2021b; and references therein). The Pyrenees present a wide range of climate regimes due to the different exposure of the massifs to the main air masses and the rough orography of the region. Temperature is primarily governed by elevation, being the elevation gradient of ca. 0.6 °C per 100 m and the annual 0 °C isotherm at ca. 2750–2950 m (López Moreno and Garcia Ruiz, 2004; and references

therein). Thermal-inversions between mountain summits and valleys (most of them N-S oriented) are frequent during stable weather conditions, particularly in winter (Pagès et al., 2017).

The combination of cold temperatures during the cold season of the year and relatively abundant precipitation favours the occurrence of snow cover in most of the Pyrenean massifs for several months of the year. Snowfall patterns in the western and central areas of the southern slopes of the range are mainly controlled by NAO phases (López-Moreno, 2005). However, no significant link with NAO is found in the northern slopes during the winter months (Alonso-González et al., 2020a, 2020b). W, NW, N and NE advections control the snow accumulation on the northern slopes of the central-eastern zone, whereas precipitation shadow effects decrease the Atlantic low-pressures system influence in the eastern area (Bonsoms et al., 2021a), as well as in the valley bottoms (González et al., 2021). In addition, the climate becomes gradually more continental towards the southern slopes of the eastern range, where the snow regime shows a marked interannual variability (Bonsoms et al., 2021b). The above-mentioned climatic contrasts eventually drive the snow climatology on the mountain range. Snow accumulation increases (decreases) to the west (east), being >600 cm (< 400 cm) at ca. 1800 m (Navarro-Serrano and López-Moreno, 2017). Similarly, snow accumulation recorded on the northern slopes of the central and eastern sectors almost doubles (500 cm) the amount recorded on the southern massifs at the same elevations (Bonsoms et al., 2021a). Snow plays a key role as water reservoir for the dry season (summer), and the meltwater of the range constitutes >40% of the southern slope rivers discharge (López-Moreno et al., 2008).

3. Data and methodology

3.1. SAFRAN system and SURFEX/ISBA-Crocus – MEPRA model

The long-term analysis (> 50 years) covering the entire range performed in this study can only be done with reanalysis datasets. This is because snow studies in the Pyrenees are constrained by temporal and spatial availability of in-situ climate and snow data. In some sectors of the mountain range, such as in the high elevation areas of the southern slopes of the Pre-Pyrenees, instrumental records started in the early 2000s (e.g., Bonsoms et al., 2021b). This makes challenging comparing data in different areas. Ground-based meteorological measurements include different temporal periods and have a sparse spatial distribution (Alonso-González et al., 2020a, 2020b) with lack of records at high elevation areas (Batalla et al., 2016). In this regard, this study used the recently published reanalysis dataset of Vernay et al. (2021), consisting of modeled values from the SAFRAN meteorological analysis (Durand et al., 1999) and the SURFEX/ISBA-Crocus – MEPRA snow cover model (S2M) for each massif of the Pyrenees (Fig. 1) at hourly resolution. SAFRAN was forced with numerical weather prediction models (ERA-40 reanalysis data from 1958 to 2002 and ARPEGE from 2002 to 2020) assimilated with ground-based observations (Vernay et al., 2021) and data was gap-filled and calibrated with homogenized in-situ meteorological observations. A detailed description of SAFRAN can be found in Durand et al. (1999) with further technical details in Vernay et al. (2021). The physical bases of the S2M heat fluxes modelling can be found in Vionnet et al. (2012); whereas an accurate description of the turbulent heat fluxes calculation, based on the ISBA-ES snow scheme, is provided in Boone and Etchevers (2001). The temporal set defined in this study includes all the days since 1959 to 2020, between March and June according to the snow ablation dates defined by Bonsoms et al. (2021a).

3.2. The amount of energy available for snow ablation (Q_m)

The amount of energy available for snow ablation (W m^{-2}) was calculated as follow:
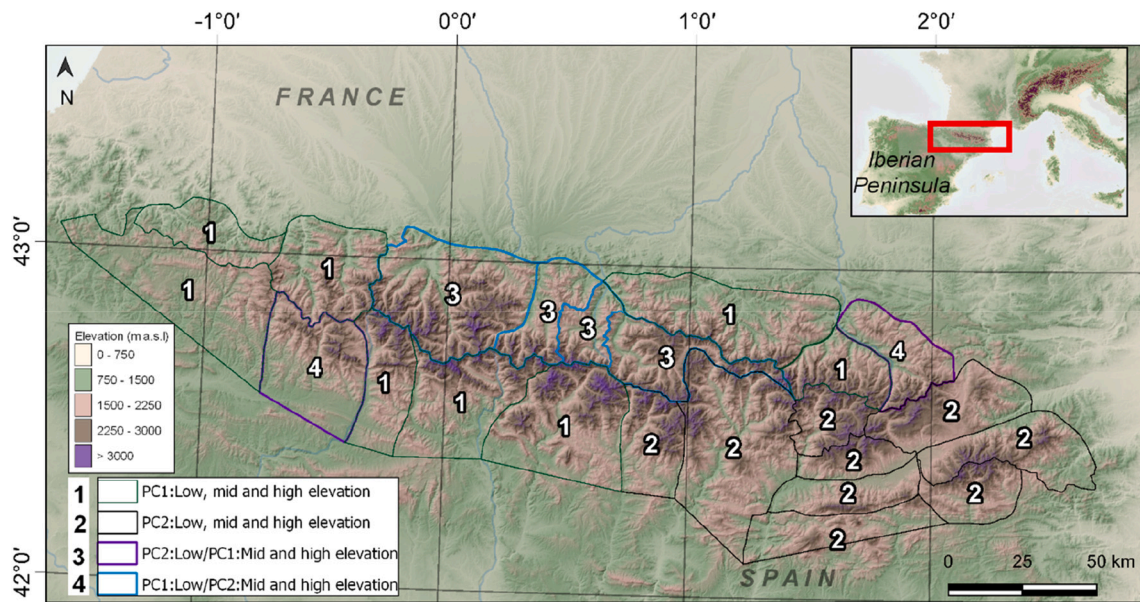
Fig. 1. Spatial distribution of mountain sectors analyzed in the Pyrenees. The PCs distribution of each massif by elevation can be consulted at Table SP1. Data of the digital elevation model was downloaded from the European Environmental Agency (https://www.eea.europa.eu/data-and-maps/data/eu-dem).

$$Q_m = Rn + H + LE + G + P \tag{1}$$

where R_n is the net radiation – the difference between shortwave (SW) and longwave (LW) radiation. H is the sensible heat flux, LE is the latent heat flux, G is the ground heat flux and P is the advection of energy by precipitation. G and P can be neglected in alpine snowpacks (e.g., Etchevers et al., 2004), specially during the snow ablation phase (e.g., Musselman et al., 2017; López-Moreno et al., 2017), simplifying the equation as follows:

$$Q_m = Rn + H + LE \tag{2}$$

3.3. Spatial regionalization of the Pyrenees according to the Q_m components

The SAFRAN system provides data by homogeneous meteorological mountain massifs every 300 m from 0 to 3600 m (Durand et al., 1999; Vernay et al., 2021). In order to retain the main Q_m variance for each mountain massif and elevation, we applied a Principal Component Analysis (PCA) on the Q_m components (SW and LW up and down, H and LE). PCA is a broadly used statistical technique for multifactorial analysis in hydro-climatological and snow-related studies (e.g., López-Moreno et al., 2020a, 2020b; Matiu et al., 2020). The PCA has been performed for each massif and for each specific low, mid and high elevation. The PC loadings for each massif and elevation can be consulted in the supplementary material (Table SP1).

3.4. Circulation weather types (CTs)

We performed a synoptic classification based on the extreme score's methodology, defined at Esteban et al. (2005), included in the COST733 project (Philipp et al., 2014) and implemented with the SynoptReg R package (Lemus-Canovas et al., 2019). This method performs a S-mode matrix with varimax rotation over a set of retained PC components. In this case, we retained 4 PCs (explaining 70.4% of the variance) based on the slope change of the Scree Test (Cattell, 1966). The explained variance of each component can be consulted in the supplementary material (Table SP2). Following the method, the 4 PCs derive in 8 CTs, since the days are classified using a K-Means clustering algorithm depending on the maximum positive and negative correlation values. Data used were daily Surface Level Pressure (SLP) and 500 hPa Geopotential Height

(Z500) from the NCEP/NCAR Reanalysis 2 (Kalnay et al., 1996). We also added the Temperature at 850 hPa (T850) and the Relative Humidity at 850 hPa (RH850) in order to discuss the results and provide a better analysis of each CT. Data for the 30°N-60°N and 30°W-10°E domain were used at 2.5° resolution, from 1959 to 2020 during the ablations season (March to June).

3.5. Trend analysis

Trends were calculated using the non-parametric Mann-Kendall trend test (Tau MK; Mann, 1955; Kendall, 1955) and the Sen's slope (Sen, 1968). The Tau MK is a broadly used trend analysis method. However, it does not detect autocorrelation in the data, which can lead to false positive trends (Hamed and Rao, 1998). For this reason, the data time series were detrended with the Sen's slope and the lag-1 autocorrelation coefficient, applied with the Modifiedmk R package (Patakamuri et al., 2017). Trends were considered statistically significant when the p-value is ≤ 0.05.

3.6. Contribution of the atmospheric circulation changes in the Q_m

We quantified the contribution of the atmospheric circulation changes on the Q_m following the regression method proposed by Ceppi et al. (2012) and Jansa et al. (2017), among other works. Here, we performed a Random Forest (RF) regression. The RF is a non-parametric algorithm based on ensembles trees and bootstrap aggregation, which capture the non-linearities of the data and is robust to outliers (Breiman, 2001). In the RF regression, a group of trees is developed using multiple decision trees, trained from random subsets of the data. The predicted values of the RF were the result of the arithmetic average of all the tree predictions (M). The M trees {$M_1(X), M_1(X), …, M_K(X)$}, where X = {x1, x2, …, xβ}, is a β-dimensional input vector that creates a forest. The ensembles generate P values that correspond to the tree Y_p (p = 1, 2, …, P). The regression RF can be calculated as follows:

$$f(x) = \frac{1}{M} \sum\nolimits_{m=1}^{M} M_k(x_j) \tag{3}$$

The independent variables were the pressure data (SLP and Z500) PC loads of the CT days related with snow ablation (Fig. 2), whereas the dependent variable was the Q_m. The SLP and Z500 model was trained
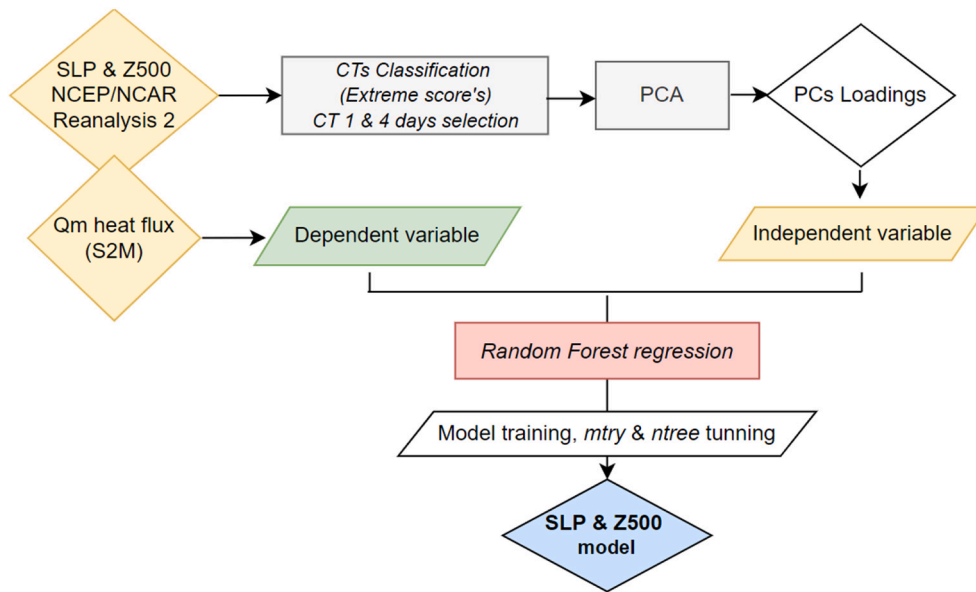
Fig. 2. Flow diagram to build the SLP and Z500 model using the RF algorithm.

with a random selection of the 70% of the dataset. The two hyper-values of the RF, the amount of the predictors evaluated in each node (*mtry)* and the number of trees (*ntree*) of a random sample, were tunned based on a grid-search with a 10-fold cross validation. The *mtry* ranged from 1 to 10 in steps of 1 and the different *ntree* values tested were 50, 100, 200, 400 and 800. The accuracy metrics of the parameter tunning can be consulted in the supplementary material (Table SP2). We evaluated the accuracy and performance of the SLP and Z500 model against the Q_m values of the entire dataset using four statistical metrics: residual (Eq. (4)), mean absolute error (MAE; Eq. (5)), root mean square error (RMSE; Eq. (6)) and coefficient of determination (R^2; Eq. (7)). Residual, MAE, RMSE and R^2 are expressed as:

$$\text{Residual} = E_i - O_i \tag{4}$$

$$\text{MAE} = N^{-1} \sum_{i=1}^{N} |E_i - O_i| \tag{5}$$

$$\text{RMSE} = \sqrt{\frac{1}{N} \sum_{i=1}^{N} (E_i - O_i)^2} \tag{6}$$

$$R^2 = \left[\frac{\sum_{i=1}^{N} (O_i - \overline{O}) \sum_{i=1}^{N} (E_i - \overline{E})}{\sqrt{\sum_{i=1}^{N} (O_i - \overline{O})^2} \sqrt{\sum_{i=1}^{N} (E_i - \overline{E})^2}} \right]^2 \tag{7}$$

where N is the number of the samples, O_i is the Q_m value and E_i is the predicted Q_m by the SLP and Z500 model. $\overline{O}$ is the average Q_m, and $\overline{E}$ is the average Q_m predicted by the PC loadings of SLP and Z500 model. Low residual, MAE and RMSE values are inversely related with higher model accuracy. On the contrary, high R^2 values are related with higher performance. The RF algorithm application was carried out with the randomForest package (Liaw and Wiener, 2012), whilst the algorithm tunning was performed with the Caret package (Kuhn, 2014) both from R Studio (R Core Team, 2018).

4. Results and discussion

We present a characterization of the Q_m components during the snow ablation phase in the Pyrenees, and subsequently we compare the results

with the heat fluxes observed in other mountain ranges. Then, we analyze the spatiotemporal trends of the Q_m for the period 1959–2020. We also quantify the impact of the CTs on the Q_m components. Finally, we determine if the Q_m trend can be linked with changes of the main synoptic patterns associate with snow ablation. To this end, we performed a regression, where the pressure data (SLP and Z500 model) is the independent variable and the Q_m is the dependent one.

4.1. Characterization of the Q_m heat fluxes

The main driver of Q_m is Rn (59%, over the total Q_m), followed by LE (35%) and H (6%; Table 1). Turbulent heat fluxes slightly decrease to the west area), corresponding mainly with PC1 (Fig. 3). The massifs associated to PC1 correspond mostly to the western Pyrenees and show less exposure to radiation and sublimation. Changes in the percentage of contribution of each Q_m component are observed depending on the elevation range. The ratio of Rn over the Q_m increases with elevation (Table 1 and Fig. 4). The reduction of H and LE with elevation is explained by the vertical lapse rates of air temperature and vapor pressure (e.g., Hock, 2005).

In accordance with our results, in-situ meteorological observations revealed that Rn is the most important energy flux of the snowpack at 2400 m in the central Pyrenees, decreasing towards the southern slopes in the western fringe of the range (López-Moreno et al., 2017). In the semiarid Sierra Nevada (2500 m; South Iberia) evaposublimation constitutes a 24–33% of the seasonal snow ablation (Herrero and Polo,

Table 1

Average daily heat fluxes (W/m²) grouped by PC and elevation. The numbers in parentheses are the percentages of each heat flux over the total Q_m. Percentages are calculated by dividing the heat fluxes for the total Q_m and multiplying by 100.

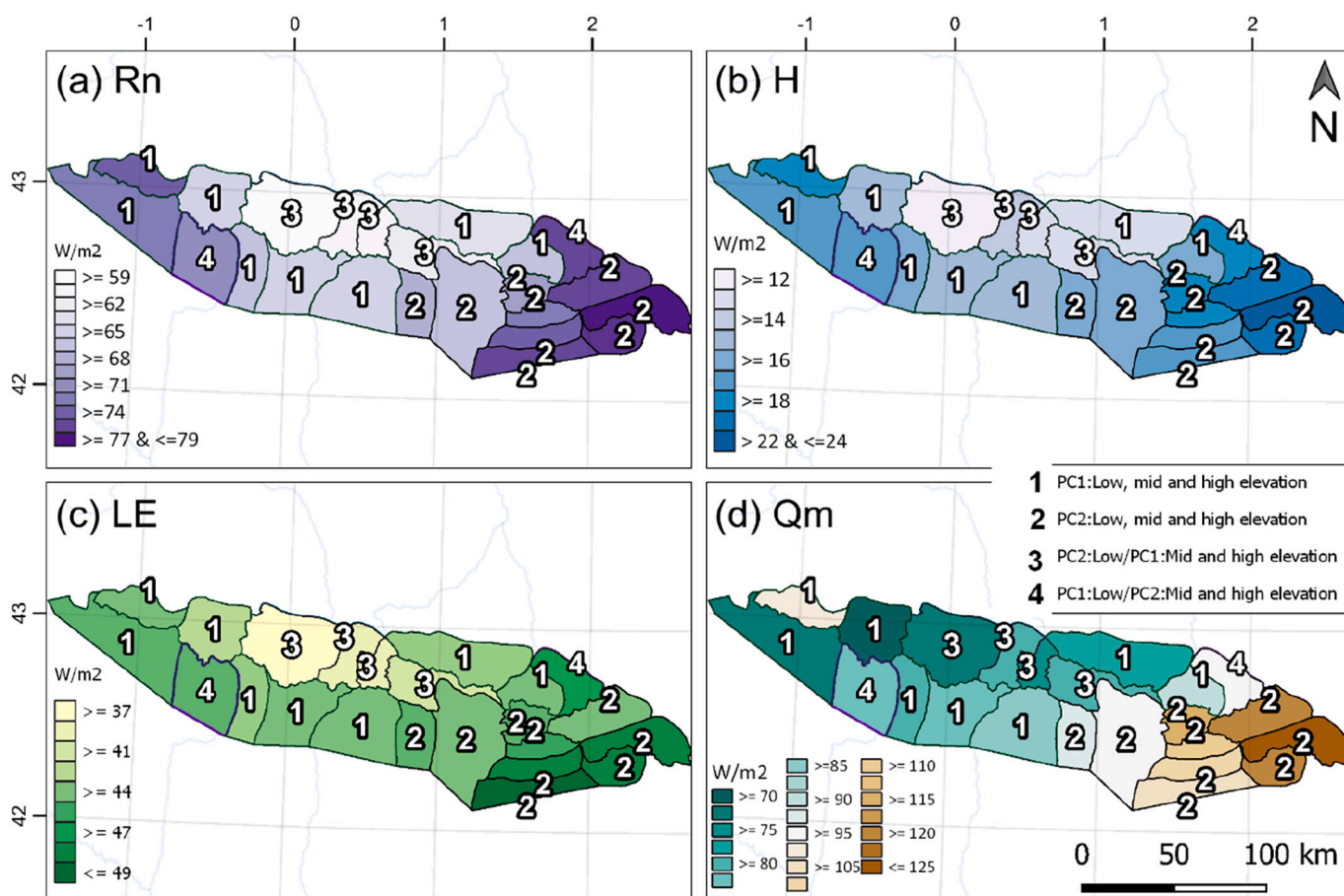|	PC1			PC2		
	Low	Mid	High	Low	Mid	High
Rn	66.8 (54%)	56.7 (60%)	31.5 (49%)	73.0 (53%)	63.5 (56%)	38.8 (58%)
H	15.2 (12%)	5.7 (7%)	−16.0 (25%)	18.7 (14%)	14.6 (13%)	−5.9 (9%)
LE	42.6 (34%)	31.3 (33%)	17.0 (26%)	46.4 (34%)	35.5 (31%)	22.7 (34%)
Q_m	124.5	93.7	32.5	138.1	113.6	55.6

Fig. 3. Spatial distribution of the average (a) Rn, (b) H, (c) LE and (d) Q_m heat fluxes.

2016). Similar percentages have been measured in the Atlas Mountains at 2300 m, where the H and LE accounts for 10% and 30%, respectively, of the seasonal snow ablation (Boudhar et al., 2016). In the western United-States and in the Australian Alps, Rn was found to be also the main driver of snow ablation (Musselman et al., 2017; Bilish et al., 2018). The latter have demonstrated that LW radiation is the main component of Rn for snow ablation (from 75 to 86% over the total snow ablation); with net SW radiation accounting for 8–14%. In the same study area, Schwartz et al. (2020) showed different Q_m contributions on the winter snowpack depending on the CTs. In their study, they found that the dominant energy source for ablation is Rn, contributing a 53–73% of the mean daily energy flux; followed by H that contributed a 16–44% during warm and dry synoptic configurations. By contrast, in Tascadero 3500 m (central Chilean Andes) sublimation constitutes 39% of the seasonal snow ablation loss (López-Moreno et al., 2017).

4.2. Spatiotemporal trends of the Q_m

The daily average Q_m for both PCs between 1959 and 2020 shows an increasing trend. The spatial distribution of the trends shows a different pattern along the Pyrenees (Fig. 5). The highest Tau MK and statistically significant values are observed in the massifs that conform PC1 (Tau MK = 0.25, Sen's Slope = 0.08, p-value $\leq$ 0.05), decreasing towards the eastern massifs that conform PC2 (Tau MK = 0.16, Sen's Slope = 0.23, p-value >0.05).

The temporal evolution of the average daily Q_m during the 60 years shows three 20-years length periods with contrasted trends (Fig. 6). The first period from 1959 to 1980 recorded lower-than-the-average daily Q_m values and a statistically significant negative trend of the average daily Q_m PC1 (Tau MK = −0.55, Sen's Slope = −2.08, p-value $\leq$ 0.01)

and PC2 (MK = 0.59, Sen's Slope = −2.31, p-value $\leq$ 0.01). This trend was probably caused by the solar dimming period (Wild, 2009) that triggered a negative trend in all Q_m components (except for LW down at low and mid elevations; Fig. 7).

The following two decades (1980–2000) showed a progressive increase of the seasonal average of daily mean Q_m for both PCs. An abrupt increase of the daily average Q_m was observed between 1980 and 2000 (Fig. 6). The upward trend is statistically significant for PC1 (Tau MK = 0.39, Sen's Slope = 1.54, p-value $\leq$ 0.05) and PC2 (Tau MK = 0.42, Sen's Slope = 1.70, p-value $\leq$ 0.01). The Q_m trends concurred with the sudden climate warming recorded in the Northern Hemisphere (Sippel et al., 2020) during the so-called regime shift period (1980 – 1995s; Marty, 2008; Reid et al., 2016). Those years were characterized by a global brightening phase (Wild, 2009) combined with positive anomalies in the large-scale low-atmospheric climate modes, such as the NAO and the Pacific Decadal Oscillation (e.g., Yasunaka and Hanawa, 2002). The compounding effects of natural climate factors (i.e., the recovery after El Chichón volcanic eruption) and increasing anthropogenic greenhouse gases emissions caused a cascade of parallel changes in the entire global ecosystem (Reid et al., 2016). In the Iberian Peninsula, the increase of atmospheric aerosols and the reduction of the cloudiness triggered an upward trend of SW (+ 3.8 Wm^{-2} decade^{-1}; Sanchez-Lorenzo et al., 2013). The regime shift impacted in the snow season of the Pyrenees, and during the 1980s the minimum HS records were reached (mean value of 1930–1990; Vilar-Bonet and Salvador-Franch, 1996). The recurrent positive phases of the NAO translated into negative snowfall anomalies and snow-scarce seasons (López-Moreno, 2005). The above-average Q_m (Fig. 6) are in accordance with statistically significant rates of warming in NE Iberia during the spring months (+ 0.66 °C decade^{-1}, 1920–2006; El Kenawy et al., 2012). The evolution observed
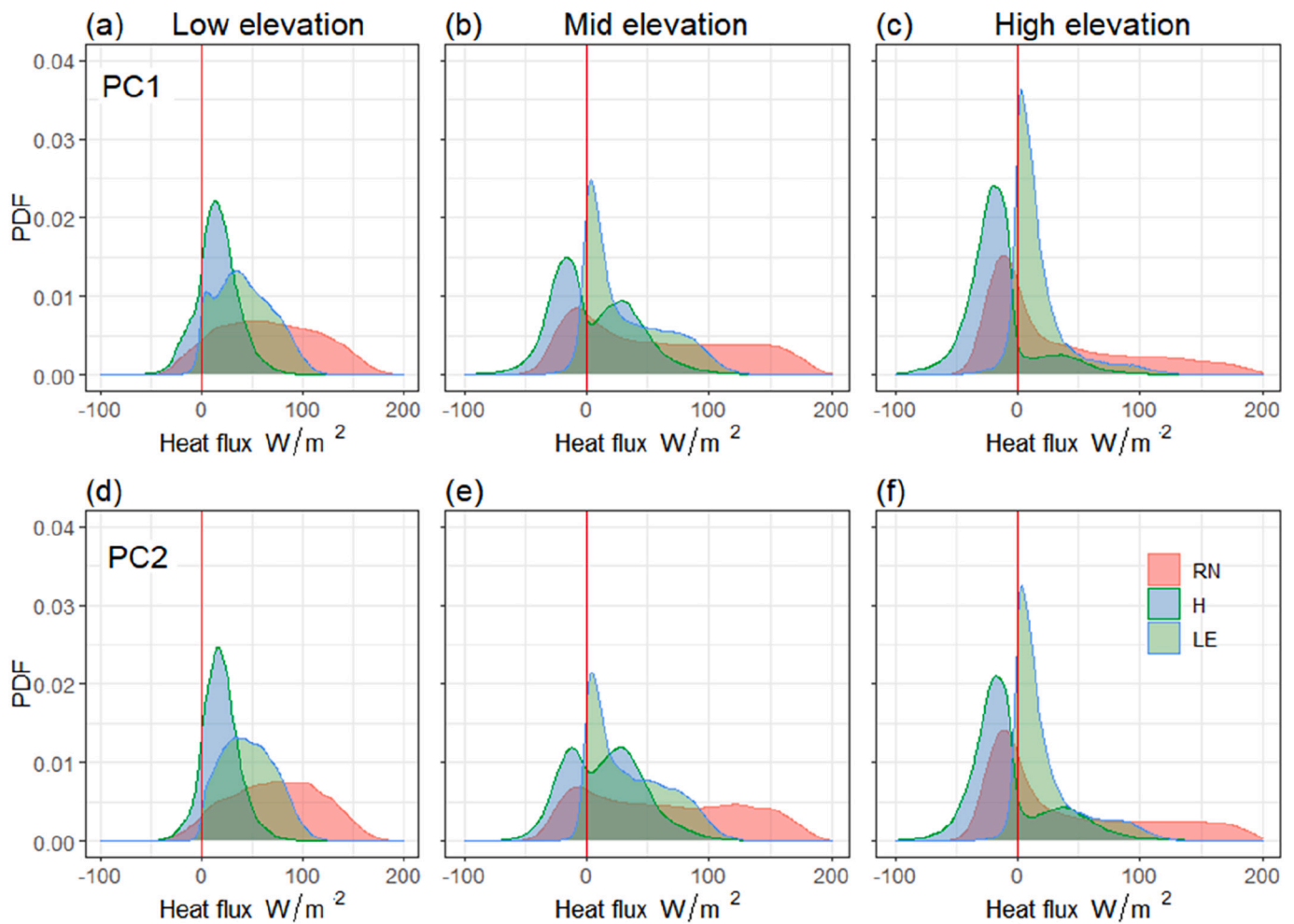
Fig. 4. Probability Density Function (PDF) of the Q_m components for (a, d) low, (b, e) mid and (c, f) high elevations. The upper row (a, b, c) corresponds to PC1 and the bottom row (a, b, c) to PC2.
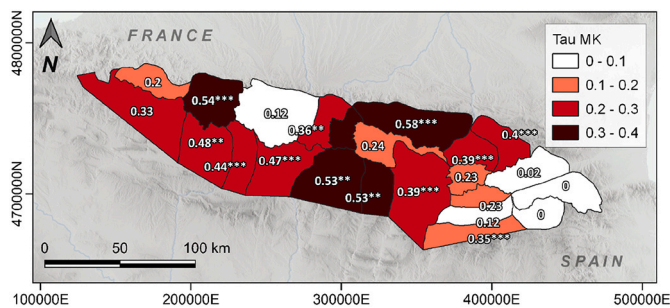

Fig. 5. Spatial distribution of the Tau MK daily average Q_m for the period 1959–2020 (shaded). The numbers represent the Sen's Slope, and the asterisks the p-value ($\leq 0.01 = ^{***}$; ≥ 0.01 and $\leq 0.05 = ^{**}$; ≥ 0.05 and $\leq 0.1 = ^{*}$).

in the Pyrenees was also detected in other European mountain ranges, such as the Alps (e.g., Scherrer and Appenzeller, 2006; Marty, 2008; Durand et al., 2009; Valt and Cianfarra, 2010; Klein et al., 2016; Marcolini et al., 2017; Schöner et al., 2018; Matiu et al., 2020; Vorkauf et al., 2021). Here, the sudden increase of temperature observed since the 1980s (Begert et al., 2005; Ceppi et al., 2012), accentuated during spring (+ 0.84 °C decade^{-1}, 1975–2004; Rebetez and Reinhard, 2008) led a reduction of 20–60% of the snow days at <1800 m (mean value of 1947–2007; Marty, 2008). The period 1980–1995 recorded the highest negative HS anomalies of the 20th century; this pattern was observed in

the Swiss (e.g., Scherrer and Appenzeller, 2006; Klein et al., 2016; Vorkauf et al., 2021), Austrian (Schöner et al., 2018), Italian (Valt and Cianfarra, 2010) and French Alps (Durand et al., 2009). Therefore, the similar evolution for the period 1980–2000 between the Alps and the Pyrenees probably suggests the existence of a relatively synchronous regional-scale pattern in western Europe (Marty, 2008).

Unlike the two previous periods, Q_m trends for the period 2000–2020 have drawn a tendency towards stabilization (Fig. 6). Moderate Sen's slopes in combination with non-statistically significant changes are observed for both PCs. A positive average daily Q_m trend was found for PC1 (Tau MK = 0.07, Sen's Slope = 0.30, p-value >0.05), whereas a slightly negative one was observed for PC2 (Tau MK = −0.02, Sen's Slope = −0.14, p-value >0.05). The higher rates of change are related to the negative SW trend, which is consistent with the negative all-sky downward surface solar radiation trend during spring in eastern Iberia (1994–2010) due to cloud radiative effects (Sanchez-Lorenzo et al., 2017). In the Pyrenees, the regime shift was followed by two decades with positive anomalies of W advections during the winter months that triggered an absence of winter temperature trends (OPCC-CTP, 2018). An upward trend in snow days at ca. 1000 m (Buisán et al., 2014) as well as positive HN trends in the elevated areas of the eastern sector of the range (Bonsoms et al., 2021a) were also observed. Similar climate patterns have been found in the Alps, where the increase of the cyclonic CTs during winter (Ceppi et al., 2012) have caused a decrease of the seasonal temperature (−0.37 °C/decade^{-1}, 1989–2016; Saffioti et al., 2016) and winter HS values have recovered since the late 1990s up to 2020 (Matiu
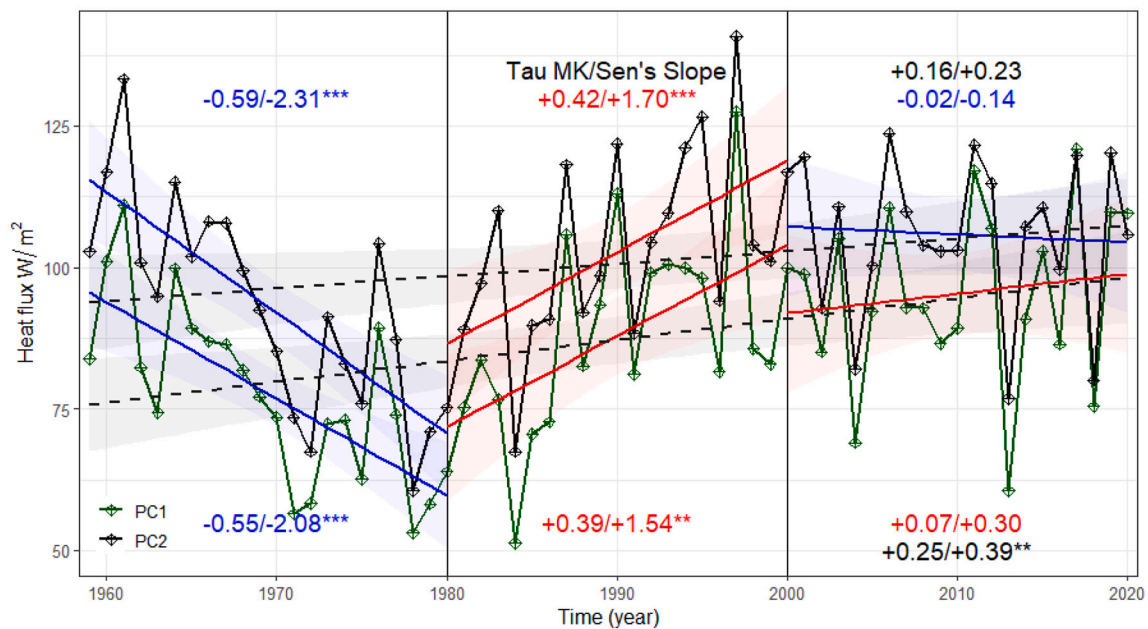
Fig. 6. (a) Evolution of the seasonal average of daily Q_m (W/m^2) during the ablation season, from 1959 to 2020 and grouped by PCs. The numbers correspond to the Tau MK/Sen's slope. *p*-values ≤ 0.01 are indicated as ***; ≥ 0.01 and ≤ 0.05 as **; ≥ 0.05 and ≤ 0.1 as *. The colored area shows the confidence intervals at 0.95 of the regression.

et al., 2020). Hence, changes in atmospheric circulation have potentially masked higher rates of change, and no clear trends in snow melt dates were found since the end of the regime shift (Vorkauf et al., 2021).

The increase in Q_m and the consequent shortening of the snow season since the 1980s is more pronounced at mid to high elevations, with no significant changes observed at low elevations (Fig. 8). Comparison between the period 1959–1980 and the 2000–2020 reveals that the first positive Q_m day was on average 22 (12) days earlier at mid (high) elevation. The daily mean Q_m follows the same increasing pattern by elevation. The average daily Q_m for the period 2000–2020 at high elevation was almost the double than the recorded for the period 1959–1980 (57.8 W m^{-2} vs 30.8 W m^{-2}, respectively; Fig. 8 and Table 2). Increasing trends in Q_m since the 1960s are in accordance with the statistically significant increase in temperature at spring, as opposed to the non-statistically significant negative temperature trends observed during winter (El Kenawy et al., 2012; OPCC-CTP, 2018; López-Moreno et al., 2020a, 2020b). The lack of Q_m change in low elevation areas are explained by the fact that snow melt starts in the last weeks of winter, and the snowpack is inexistent or ephemeral at spring (Bonsoms et al., 2021a). Therefore, the Q_m trends for low elevation areas presented in this work provide more evidence of slower snowmelt rates in shallower snowpacks (Musselman et al., 2017). Given that Q_m at high elevations is governed by Rn, the upward (downward) trend observed for LW (albedo) have probably implied a chain of positive snow-albedo feedbacks, that have potentially elevated the 0 °C isotherm to higher elevations. Snow-albedo feedbacks, mainly observed in spring (e.g., Giorgi et al., 1997), have been attributed to increasing rates of climate warming found during the spring months (ca. 1500 m; Ceppi et al., 2012).

One of the consequences associated with Q_m trends is the glacier recession recorded in the Pyrenees in recent decades. Glacier ablation followed a rate of 21.0 hm^2 loss year^{-1} between 1984 and 2008; however, the slowdown in the Q_m rate observed reported here since the 2000s has potentially decreased the rate, resulting in 8.1 hm^2 loss year^{-1} between 2008 and 2016 (Rico et al., 2017). The increase in LE, and the consequent offset of H at low elevations (Fig. 7), is in agreement with the upward rate of evapotranspiration (López-Moreno et al., 2008). Snow evaporation increases implies meltwater decreases, and therefore less runoff. In this sense, a decrease in the Pyrenean rivers streamflow have

been observed since the end of the century for both the Northern and Southern slopes of the Pyrenees (Renard et al., 2008). This trend has been attributed to the earlier snowmelt onset (López-Moreno et al., 2008; Morán-Tejeda et al., 2014), the denser forest cover in the river's headwaters (Beguería et al., 2003; López-Moreno et al., 2006; Gallart et al., 2011) and the decrease in winter snowfall during the second half of the 20th century (López-Moreno, 2005; López-Moreno et al., 2008). The increasing Q_m trends and the earlier positive Q_m dates pointed out in this work suggest an increase (decrease) of the winter (spring) season streamflow (López-Moreno et al., 2008). Changes in the snow melting timing have already been linked with the earlier peak flow observed in Iberian rivers during the second half of 20th century (Morán-Tejeda et al., 2014). These hydrological changes imply a decrease in the energy available for hydropower, but also a decrease of land-irrigated sources and socioeconomic uses in the downstream areas. Given that temperature, instead of the accumulated winter precipitation, is the key parameter that determines the snow duration and SWE peak in the Pyrenees (Alonso-González et al., 2020a, 2020b), projected climate warming for the mid 21th century in this mountain range (> 1 °C; Amblar-Francés et al., 2020) will likely amplify the Q_m trends observed, as well as the cascade of effects discussed here.

4.3. The impact of atmospheric circulation changes on the snow ablation phase

The CTs types that rule the atmospheric circulation variability over the study area are presented in Fig. 9. From March to June, the majority of the days are clustered with CT 1 (22.3%), followed by CT 4 (14.9%) and CT 6 (12.9%; Table 3).

In all of the CTs, the largest contribution of Q_m is Rn. CT 3, 6 and 8 represent the advection of Atlantic low-pressure systems over the mountain range. Cold conditions and lower than average RH850 generate low rates of Q_m and negative H fluxes at high elevation. Fig. 9 (b) shows the spatial concentration of wet air masses in the western Iberian Peninsula during those events, becoming dry towards the east due to orographic effects. CT 3 represents a W flow over the Pyrenees and CT 6 is a deep-low cyclonic system established over NW Iberia, with SW a mild flow over the Pyrenees. Finally, CT 8 brings polar air masses
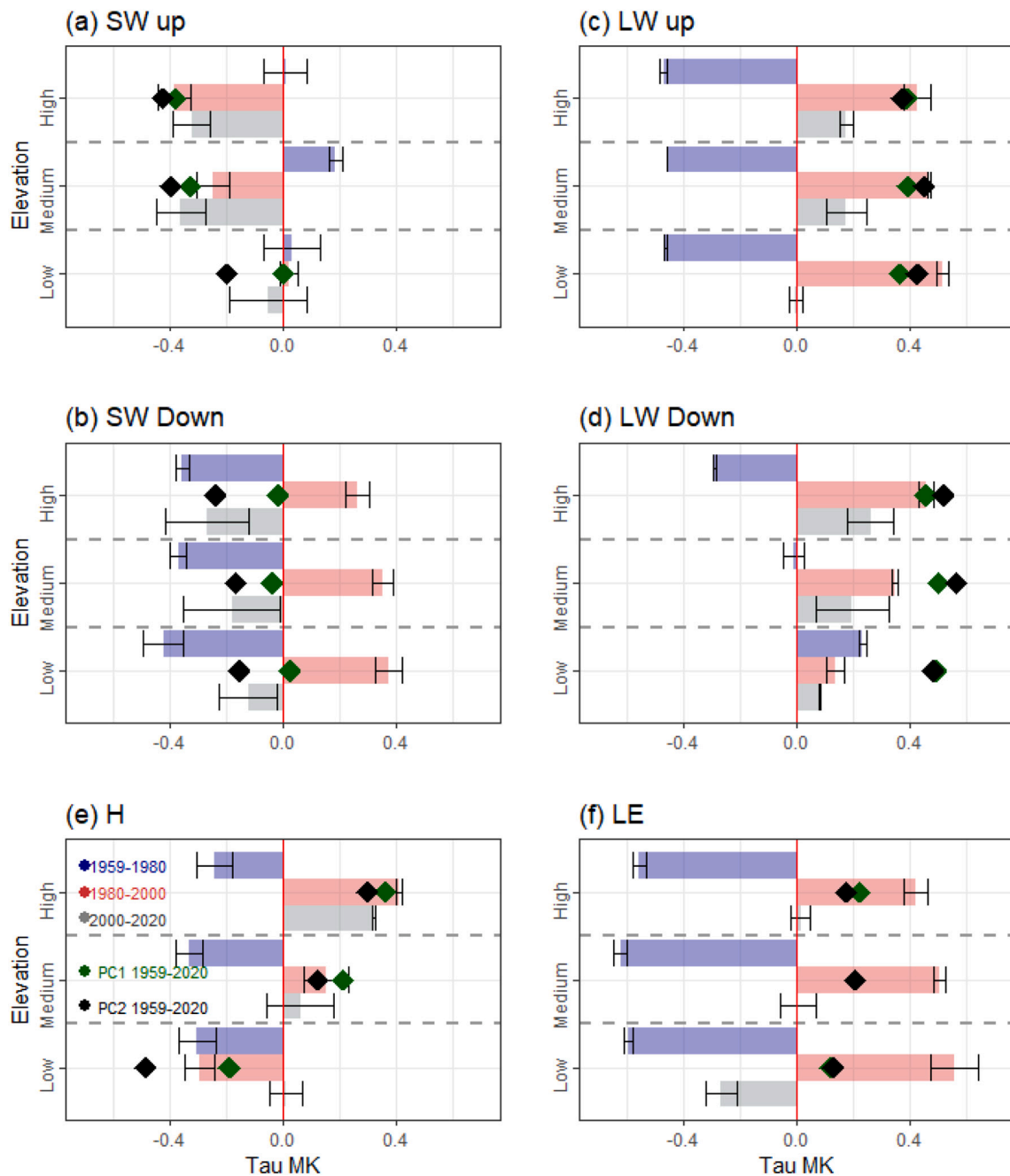
Fig. 7. Tau MK trends of the Q_m components between 1959 and 2020 grouped by elevation. Each bar shows the average of both PCs for elevation and 20-year temporal period, whereas the max and the min ticks are the values for each PC. The 60-year trends are showed with green and black squares for PC1 and PC2, respectively. (For interpretation of the references to colour in this figure legend, the reader is referred to the web version of this article.)

with NW flow and the coldest temperatures over the study area. Those CTs often produces precipitation, instead of positive Q_m and snow ablation conditions. CT 3 and 6 are associated with high amounts of snow over the southern slopes of the western and central Pyrenees (e.g., López-Moreno and Serrano-Vicente, 2006), whereas CT 6 contribute to positive HN and torrential rainfall in the southern slopes of the eastern Pyrenees (Bonsoms et al., 2021b; and references therein). CT 8 brings the highest contribution of snowfall on the northern slopes of the high elevation areas of the western and central (Navarro-Serrano and López-Moreno, 2017), central-eastern (Esteban et al., 2005) and eastern Pyrenees (Bonsoms et al., 2021a).

The synoptic configurations of CT 2, 5 and 7 represent the extension of an Atlantic (CT 2 and 5) and continental (CT 7) anticyclone systems

providing cold and stable snowpack conditions. CT 2 represents a cluster of synoptic configurations determined by the displacement of huge anticyclonic system placed over the British Isles. There is a N flow over the Pyrenees with colder than average T850. CT 5 is a similar configuration, with the high-pressure area displaced to the S and bringing dry air masses. Finally, CT 7 events show the extension of a high-pressure system over the whole continental Europe providing the driest air masses over the study area. The lowest daily average Q_m in the Pyrenees is observed during these synoptic configurations, which in turn trigger negative H fluxes at high elevations (H = -24 W/m^2 and -31 W/m^2, for CT 2 and 5, respectively).

CT 1 and 4 synoptic events are characterized by a low-barometric gradient over the Iberian Peninsula. Very stable weather conditions
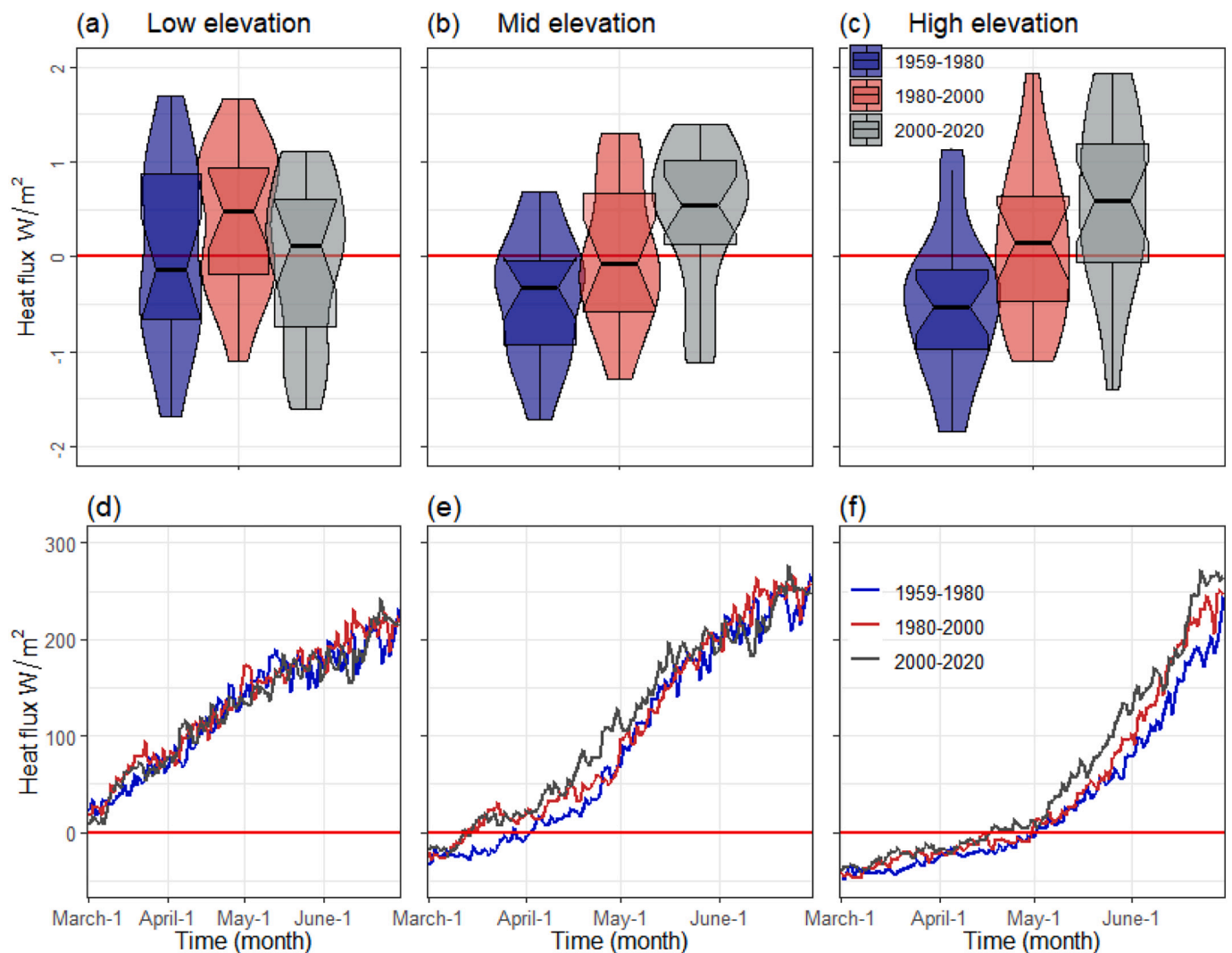
Fig. 8. Daily Q_m anomalies grouped by temporal period, for (a) low, (b) mid and (c) high elevation (upper row). Anomalies were calculated by (i) average the Q_m of the entire temporal period, calculate the difference between (ii) the average Q_m for the three 20-year periods and the average Q_m of the entire temporal period, (iii) divide the difference by the standard deviation Q_m of the entire temporal period. The bottom row shows the time series of the daily average of Q_m for the three temporal periods at (d) low, (e) mid and (f) high elevation.

Table 2
Average values of the daily Q_m (W m^{-2}) grouped by temporal period and elevation.

Daily average Q_m	Low	Mid	High
1959–1980	127.6	94.0	30.8
1980–2000	134.5	105.7	44.2
2000–2020	128.0	113.3	57.7

prevail, in combination with by the advection of hot and dry SE air masses. The CT 1 brings the highest T850 of the catalogue of CTs, and presents also the highest values of Q_m for all the elevation ranges. During both configurations (CT 1 and CT 4), the average daily Q_m is fourfold the average (Fig. 10). Those synoptic configurations represent the majority ($>$ 50%) of the days with positive Q_m. The relative contribution of CT 1 and CT 4 over the snow ablation days increases with elevation, without significant differences between PC1 and PC2 (not figure shown). The anticyclonic conditions over the Pyrenees guarantees plenty of solar radiation and clear sky conditions (Rn = 58%) with a high sublimation rate (LE = 30%) together with significant water losses due to evaporation (H = 12%).

In the Pyrenees, HS is affected by significant decadal and internal

climate variability (e.g., López-Moreno et al., 2020a, 2020b). Consequently, quantifying the role of the atmospheric changes over the seasonal Q_m is crucial in order to separate the atmospheric circulation changes from other physical processes affecting the Q_m trends. Fig. 11 show the time series of the predicted Q_m values by the SLP and Z500 model and the Q_m values. Accurate results were found between the SLP and Z500 model and the Q_m values during the days with higher and positive ablation rates (CT 1 and 4; MAE = 12.0 W/m^2, RMSE = 15.0 W/m^2). The data suggest that atmospheric circulation changes can explain most of the variability (R^2 = 75%) of the seasonal Q_m during the days with higher rates of Q_m flux (CT1 and CT4).

Therefore, the positive Q_m trends (Fig. 11; Figure SP1) have been driven by the statistically significant positive trend in the frequency of CT 1 (Tau MK = 0.32, Sen's slope = 0.18, p-value $<$0.01; Table 3), the non-variation in the frequency of CT 4 and the non-statistically reduction of the Atlantic low-pressure systems (CT 3, 6 and 8). The positive frequency of the anticyclonic events has been reinforced by the warmer ($>$ 0.5 °C T850) and drier ($<$3% RH850) conditions for the period 2000–2020 (Fig. 12). At the same time, our results suggest that the negative Q_m found for PC2 between 2000 and 2020 (Tau MK = −0.02, Sen's Slope = −0.14, p-value $>$0.05; Fig. 5) has been partly determined by the negative anomaly frequency of the CT 1 during the same temporal
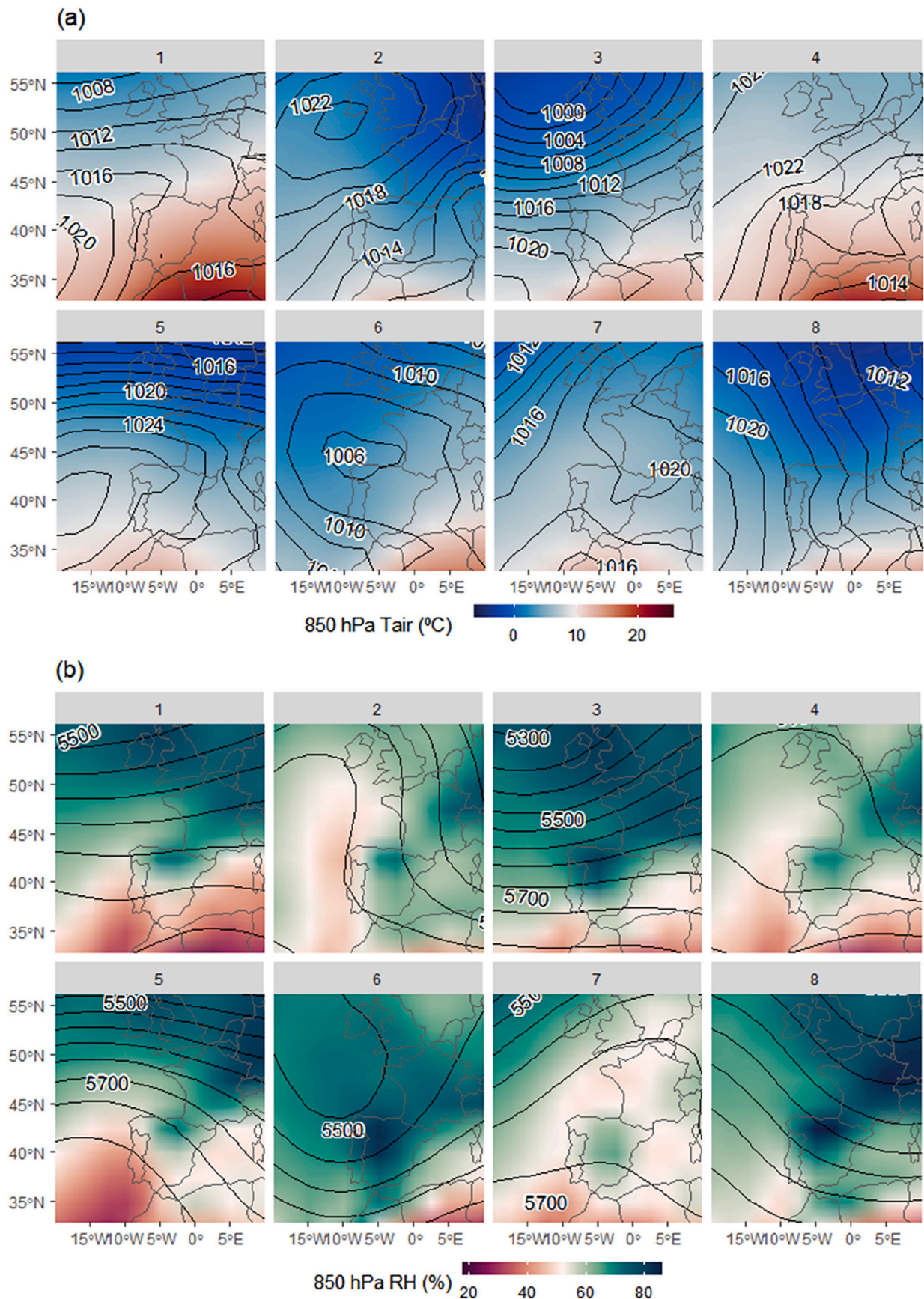
Fig. 9. CTs during the ablation season (a) Maps of the average SLP (contour lines) and T850 (shaded) grouped by CT. Same for (b) Z500 (contour lines) and RH850 (shaded).

Table 3
Frequency of days with each CT and trends during the ablation season (MAMJ).

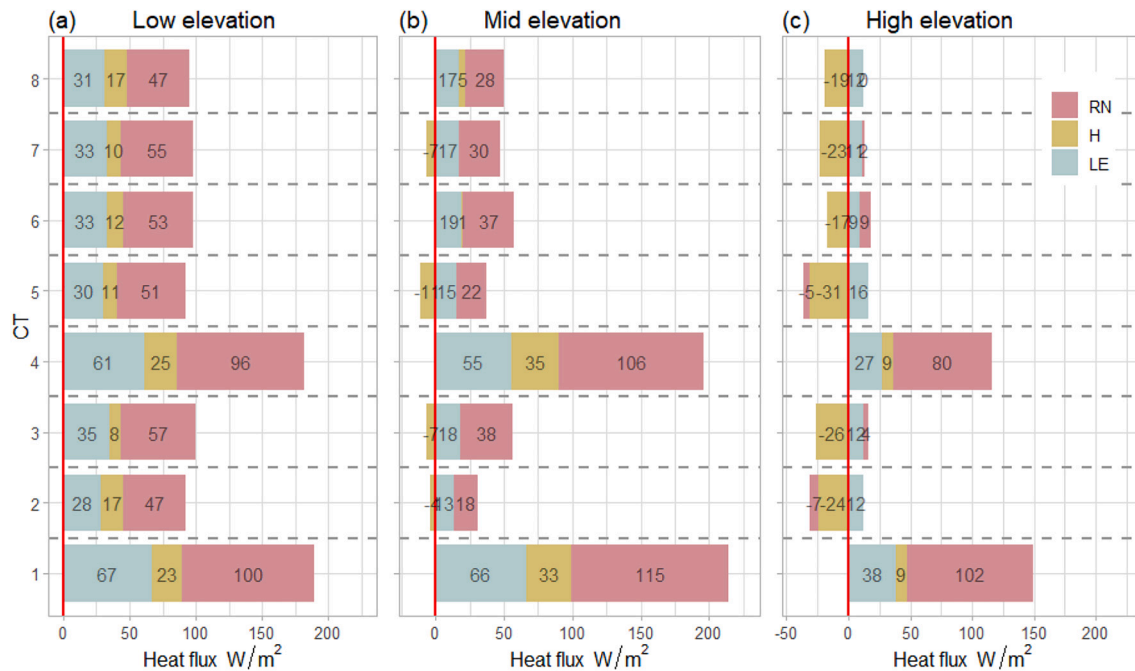| CTs	1	2	3	4	5	6	7	8
Frequency (% days)	22.28	9.96	10.83	14.91	8.54	12.94	10.58	9.96
Tau MK	0.32***	−0.20**	−0.09	0.00	−0.03	−0.07	0.19	−0.10
Sen's Slope	0.18	−0.10	−0.04	0.00	0.00	−0.03	0.09	−0.05

Fig. 10. Contribution of each Q_m component on the average daily snow ablation for (a) low (b) mid and (c) high elevation, classified by CT.
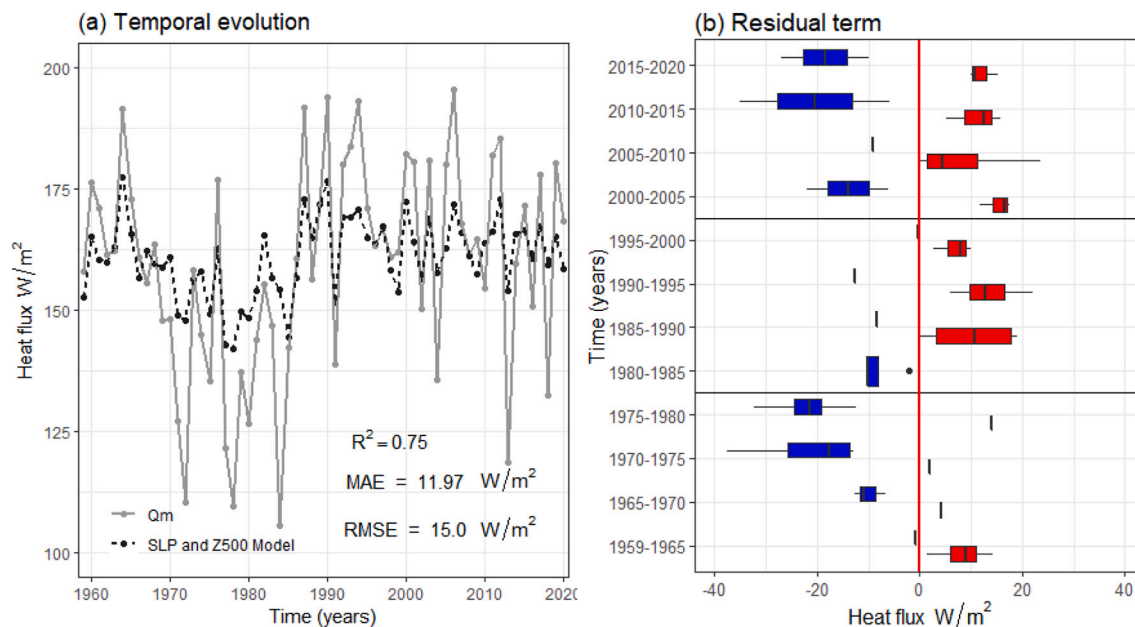

Fig. 11. (a) Time series of the SLP and Z500 model and the seasonal average of daily mean Q_m. (b) Residual term (difference between the SLP and Z500 model and the average seasonal daily mean Q_m). The blue boxes are negative differences whereas the red ones positive. (For interpretation of the references to colour in this figure legend, the reader is referred to the web version of this article.)

period (Fig. 12, b). The negative oscillation for the period 2000–2020 is potentially linked with the slowdown mean temperature trends for the Iberian Peninsula since the end of the 1990s (Vicente-Serrano et al.,

2017). The results presented in this work are in accordance with positives oscillations of the East Atlantic (EA) low-frequency climate mode, which reproduces the spatial pattern of CT 1, and rules the temperature
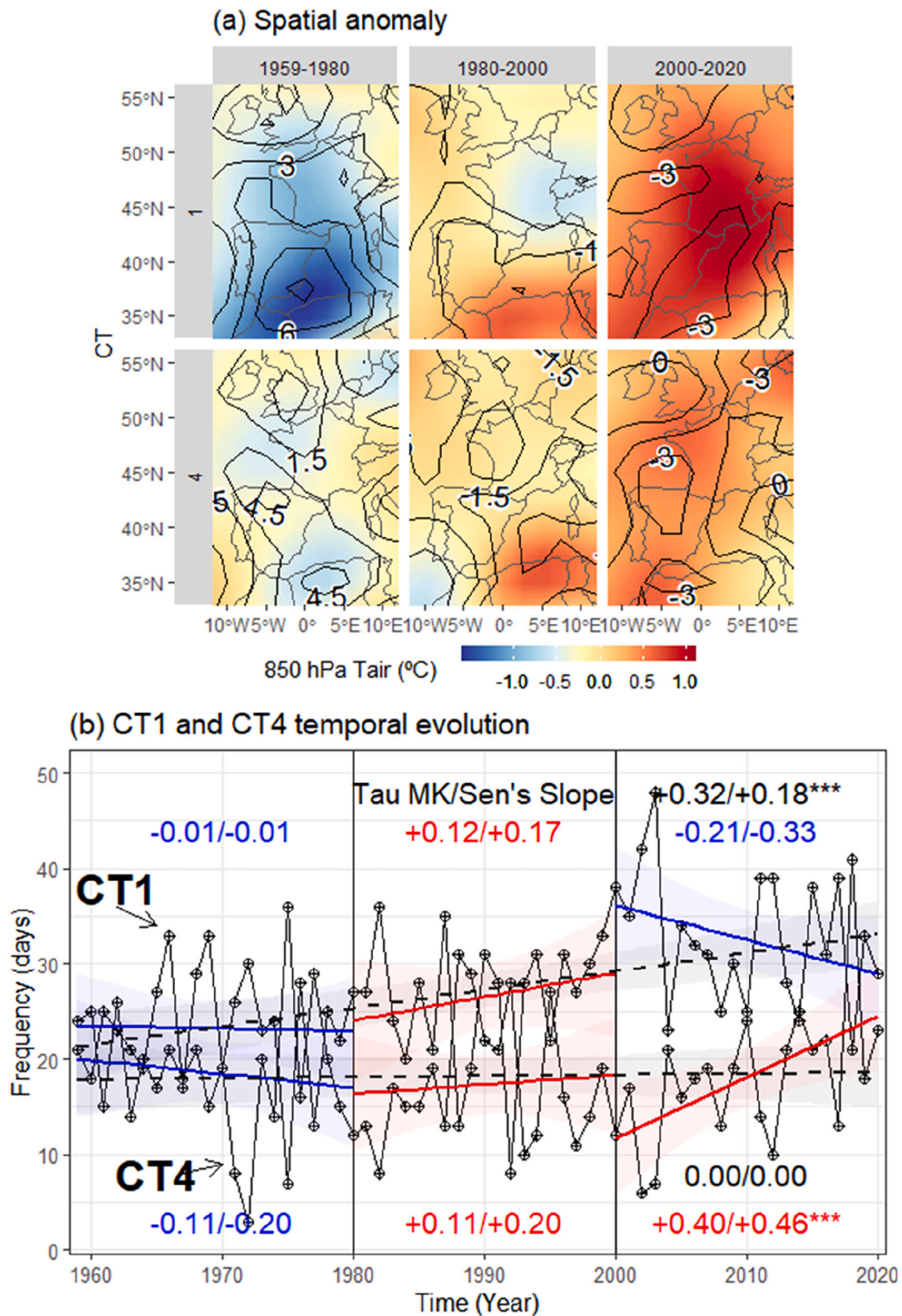
Fig. 12. (a) Spatial anomaly maps of T850 (shaded) and RH850 (labeled contours) during the CT 1 (upper row) and CT 4 (bottom row) events. The SLP is calculated by the difference of the average values recorded for the whole temporal period 1959–2020, and the average values recorded during the three 20-year periods (1959–1980, 1980–2000 and 2000–2020). (b) Temporal evolution of the CT1 and CT4 frequency, from 1959 to 2020.

during spring in the NE Iberian Peninsula ($r = 0.4$, p-value ≤ 0.05; El Kenawy et al., 2012). Atmospheric changes have been also associated with the climate warming recorded during spring (1973–2012) in Mallorca (eastern Iberian Peninsula), caused by the widening effects of the Hadley cell (Jansa et al., 2017). The increasing anticyclonic conditions observed in our work are consistent with the northern expansion of the tropical belt (ca. 4.25°) observed since the 1980s (Seidel and Randel, 2007). This shift has leaded a mid-latitude tropospheric warming and a poleward displacement of the subtropical dry zone (Hu and Fu, 2007), provoking the so-called subtropicalitzation of the Iberian Peninsula climate (De Luis et al., 2010). Future climate scenarios project an enhanced tropical belt expansion, which implies the northward displacement of the mid-latitude storms mainly during spring (Giorgi and Lionello, 2008). The related changes suggest positive Q_m trends, and an increase of the aridity conditions over the study area. The largest positive differences between the model based on atmospheric data and the Q_m values are observed since the 1980s. This suggests a decoupling of the model based on atmospheric data, due to external factors non-related with the atmospheric circulation. The attribution of other physical processes that rule the increasing Q_m (i.e., greenhouse gases emissions) is out of the scope of this article, but should be the base of forthcoming works.

5. Conclusions

Many hydrological studies in the Pyrenees have focused on the water supply side (snowfall), but less attention has been made to the energy demand fluxes (i.e., snow condensation and sublimation). In a warming atmosphere, a better understanding of the energy fluxes partitioning is crucial in order to anticipate future changes on the snow regime timing and magnitude. To this purpose, the spatiotemporal patterns of Q_m components in the Pyrenees have been examined at low, mid and high elevations and for the period 1959–2020.

The highest rate of contribution of Q_m is Rn (increasing with elevation) and LE (increasing from west to east). The Q_m temporal evolution revealed a significant decadal and internal climate variability affecting the energy fluxes. In comparison with the period 1960–2020, the period 1959–1980 was characterized by negative Q_m anomalies, followed by the 1980–2000 period, when an abrupt increase in the Q_m was found. The last period of 2000–2020 shows small and non-statistical trends, ruled by negative anticyclonic situations. The highest rates of Q_m are related with two synoptic configurations, characterized by stable weather conditions and the advection of dry and hot SE air masses. Given that regression analysis has shown that atmospheric circulation changes explain the majority of the Q_m temporal evolution, the increase in the frequency of the anticyclonic events has triggered an increase in all the Q_m fluxes. No significant Q_m changes have been observed at low elevation areas, confirming slow snow melts in shallow snowpacks. In comparison with the period 1959–1980, in mid and high elevation areas the snow ablation onset has advanced around one month for the period 2000–2020. At high elevations, the snowpack has been also exposed to a faster snow ablation daily rate, and almost the double of the Q_m per day was recorded for the same temporal period (1959–1980 vs 2000–2020).

Significant research gaps are still related with the cascading impacts in the mountain ecosystem of the hydro-climatological trends presented here. This includes, but not limits to, phenological shifts, colder surfaces under more snow-free areas or meltwater infiltration in frozen and unfrozen soils. The upward trend of snow evaporation and melting presented in this study, together with the drying conditions projected for the oncoming decades suggests a dwindling of water resources in the downstream areas. Emerging evidence has been provided for further water management strategies.

CRediT authorship contribution statement

Josep Bonsoms: Conceptualization, Methodology, Writing –

original draft, Data curation, Visualization, Investigation, Supervision, Validation, Writing – review & editing. **Juan Ignacio López-Moreno:** Conceptualization, Methodology, Supervision, Validation, Writing – review & editing. **Sergi González:** Conceptualization, Methodology, Supervision, Validation, Writing – review & editing. **Marc Oliva:** Conceptualization, Methodology, Supervision, Validation, Writing – review & editing.

Declaration of Competing Interest

The authors declare that they have no known competing financial interests or personal relationships that could have appeared to influence the work reported in this paper.

Appendix A. Supplementary data

Supplementary data to this article can be found online at https://doi.org/10.1016/j.atmosres.2022.106228.

References

Alonso-González, E., López-Moreno, J.I., Navarro-Serrano, F.M., Revuelto, J., 2020a. Impact of North Atlantic Oscillation on the Snowpack in Iberian Peninsula Mountains. Water 12, 105. https://doi.org/10.3390/w12010105.

Alonso-González, E., López-Moreno, J.I., Navarro-Serrano, F., Sanmiguel-Vallelado, A., Aznárez-Balta, M., Revuelto, J., Ceballos, A., 2020b. Snowpack Sensitivity to Temperature, Precipitation, and Solar Radiation Variability over an Elevational Gradient in the Iberian Mountains. Atmos. Res. 243, 104973 https://doi.org/10.1016/j.atmosres.2020.104973.

Amblar-Francés, M.P., Ramos-Calzado, P., Sanchis-Lladó, J., Hernanz-Lázaro, A., Peral-García, M.C., Navascués, B., Dominguez-Alonso, M., Rodríguez-Camino, E., 2020. High resolution climate change projections for the Pyrenees region. Adv. Sci. Res. 17, 191–208. https://doi.org/10.5194/asr-17-191-2020.

Batalla, M., Ninyerola, M., Trapero, L., Esteban, P., 2016. ACDA: andorran climate digital atlas (period 1981-2010). In: Map Server. Institut d'Estudis Andorrans (IEA), Universitat Autonoma de Barcelona (UAB). http://www.acda.ad.

Begert, M., Schlegel, T., Kirchhofer, W., 2005. Homogeneous temperature and precipitation series of Switzerland from 1864 to 2000. Int. J. Climatol. 25 (1), 65–80. https://doi.org/10.1002/joc.1118.

Beguería, S., López-Moreno, J.I., Lorente, A., Seeger, M., García-Ruiz, J.M., 2003. Assessing the effects of climate oscillations and land-use changes on streamflow in the Central Spanish Pyrenees. Ambio 32 (4), 283–286. https://doi.org/10.1639/0044-7447(2003)032[0283:ATEOCO]2.0.CO;2.

Bilish, S.P., McGowan, H.A., Callow, J.N., 2018. Energy balance and snowmelt drivers of a marginal subalpine snowpack. Hydrol. Process. 32, 3837–3851. https://doi.org/10.1002/hyp.13293.

Bonsoms, J., Gonzalez, S., Prohom, M., Esteban, P., Salvador-Franch, F., López-Moreno, J.I., Oliva, M., 2021a. Spatio-temporal patterns of snow in the Catalan Pyrenees (SE Pyrenees, NE Iberia). Int. J. Climatol. 41 (12), 5676–5697. https://doi.org/10.1002/joc.7147.

Bonsoms, J., Salvador-Franch, F., Oliva, M., 2021b. Snowfall and snow cover evolution in the Eastern Pre-Pyrenees (NE Iberian Peninsula) Cuad. Investig. Geogr. 47 (2), 291–307. https://doi.org/10.18172/cig.4879.

Boone, A., Etchevers, P., 2001. An intercomparison of three snow schemes of varying complexity coupled to the same land-surface model: local scale evaluation at an Alpine site. J. Hydrometeorol. 2, 374–394.

Boudhar, A., Boulet, G., Hanich, L., Sicart, J.E., Chehbouni, A., 2016. Energy fluxes and melt rate of a seasonal snow cover in the Moroccan High Atlas. Hydrol. Sci. J. 61, 931–943. https://doi.org/10.1080/02626667.2014.965173.

Breiman, L., 2001. Random forests. IEEE. Mach. Learn. 45, 5–32.

Buisán, S.T., Sanz, M.A., López-Moreno, J.I., 2014. Spatial and temporal variability of winter snow and precipitation days in the western and central Spanish Pyrenees. Int. J. Climatol. 35, 259–274. https://doi.org/10.1002/joc.3978.

Cattell, R.B., 1966. The Scree test for the number of factors. Multivar. Behav. Res. 1, 245–276. https://doi.org/10.1207/s15327906mbr0102_10.

Ceppi, P., Scherrer, S.C., Fischer, A.M., Appenzeller, C., 2012. Revisiting Swiss temperature trends 1959-2008. Int. J. Climatol. 32, 203–213. https://doi.org/10.1002/joc.2260.

De Luis, M., Brunetti, M., Gonzalez-Hidalgo, J.C., Longares, L.A., Martin-Vide, J., 2010. Changes in seasonal precipitation in the Iberian Peninsula during 1946–2005. Glob. Planet. Chang. 74, 27–33. https://doi.org/10.1016/j.gloplacha.2010.06.006.

Durand, Y., Giraud, G., Brun, E., Mérindol, L., Martin, E., 1999. A computer-based system simulating snowpack structures as a tool for regional avalanche forecasting. J. Glaciol. 45, 469–484. https://doi.org/10.1017/S0022143000001337.

Durand, Y., Giraut, G., Laternser, M., Etchevers, P., Merindol, L., Lesaffre, B., 2009. Reanalysis of 47 years of climate in the French Alps (1958–2005): climatology and trends for snow cover. J. Appl. Meteorol. Climatol. 2487–512 https://doi.org/10.1175/2009JAMC1810.1.

El Kenawy, A., López-Moreno, J.I., Vicente-Serrano, S.M., 2012. Trend and variability of temperature in Northeastern Spain (1920-2006): linkage to atmospheric circulation. Atmos. Res. 105, 159–180. https://doi.org/10.1016/j.atmosres.2011.12.006.

Esteban, P., Jones, P., Martin-Vide, J., Mases, M., 2005. Atmospheric Circulation patterns related to heavy snowfall days in Andorra Pyrenees. Int. J. Climatol. 25, 319–329. https://doi.org/10.1002/joc.1103.

Etchevers, P., Martin, E., Brown, R., Fierz, C., Lejeune, Y., Bazile, E., Boone, A., Dai, Y.-J., Essery, R., Fernandez, A., Gusev, Y., Jordan, R., Koren, V., Kowalczyk, E., Nasonova, N.O., Pyles, R.D., Schlosser, A., Shmakin, A.B., Smirnova, T.G., Strasser, U., Verseghy, D., Yamazaki, T., Yang, Z.-L., 2004. Validation of the energy budget of an alpine snowpack simulated by several snow models. Snow MIP project. Ann. Glaciol. 38, 150–158. https://doi.org/10.3189/172756404781814825.

Gallart, F., Delgado, J., Beatson, S.J.V., Posner, H., Llorens, P., Marcé, R., 2011. Analysing the effect of global change on the historical trends of water resources in the headwaters of the Llobregat and Ter river basins (Catalonia, Spain). Phys. Chem. Earth Parts A/B/C 36 (13), 655–661. https://doi.org/10.1016/j.pce.2011.04.009.

García-Ruiz, J.M., López-Moreno, J.I., Vicente-Serrano, S., Lasanta, T., Beguería, S., 2011. Mediterranean water resources in a global change scenario. Earth-Sci. Rev. 105, 121–139. https://doi.org/10.1016/j.earscirev.2011.01.006.

Gascoin, S., Hagolle, O., Huc, M., Jarlan, L., Dejoux, J.-F., Szczypta, C., Marti, R., Sánchez, R., 2015. A snow cover climatology for the Pyrenees from MODIS snow products. Hydrol. Earth Syst. Sci. 19, 2337–2351. https://doi.org/10.5194/hess-19-2337-2015.

Gilaberte-Búrdalo, M., López-Moreno, J.I., Morán-Tejeda, E., Jerez, S., Alonso-González, E., López-Martín, F., Pino-Otín, M.R., 2017. Assessment of ski condition reliability in the Spanish and Andorran Pyrenees for the second half of the 20th century. Appl. Geogr. 79, 127–142. https://doi.org/10.1016/j.apgeog.2016.12.013.

Giorgi, F., Hurell, J.W., Marinucci, M.R., 1997. Elevation dependency of the surface climate change signal: a model study. J. Climate 10, 288–296. https://doi.org/10.1175/1520-0442(1997)010<0288:EDOTSC>2.0.CO;2.

Giorgi, F., Lionello, P., 2008. Climate change projections for the Mediterranean region. Glob. Planet. Chang. 90–104 https://doi.org/10.1016/j.gloplacha.2007.09.005.

González, S., Bech, J., Garcia-Benadí, A., Udina, M., Codina, B., Trapero, L., Georgis, J.F., 2021. Vertical structure and microphysical observations of winter precipitation in an inner valley during the Cerdanya-2017 field campaign. Atmos. Res. 264, 105826 https://doi.org/10.1016/j.atmosres.2021.105826.

Grundstein, A.J., Leathers, D.J., 1999. A spatial analysis of snow-surface energy exchanges over the northern great plains of the United States in relation to synoptic scale forcing mechanisms. Int. J. Climatol. 19, 489–511. https://doi.org/10.1002/(SICI)1097-0088(199904)19:5<489::AID-JOC373>3.0.CO;2-J.

Hamed, K.H., Rao, A.R., 1998. A modified Mann-Kendall trend test for autocorrelated data. J. Hydrol. 204 (1–4), 182–196. https://doi.org/10.1016/S0022-1694(97)00125-X.

Hayashi, M., Hirota, T., Iwata, Y., Takayabu, I., 2005. Snowmelt energy balance and its relation to foehn events in Tokachi, Japan. J. Meteorol. Soc. Jpn. 83, 783–798. https://doi.org/10.2151/jmsj.83.783.

Herrero, J., Polo, M.J., 2016. Evaposublimation from the snow in the Mediterranean mountains of Sierra Nevada (Spain). Cryosph. 10, 2981–2998. https://doi.org/10.5194/tc-10-2981-2016.

Hock, R., 2005. Glacier melt: a review on processes and their modelling. Prog. Phys. Geogr. 29 (3), 362–391. https://doi.org/10.1191/0309133305pp453ra.

Hock, R., Rasul, G., Adler, C., Cáceres, B., Gruber, S., Hirabayashi, Y., Jachson, M., Kääb, A., Kang, S., Kutuzov, S., Milner, A., Molau, U., Morin, S., Orlove, B., Steltzer, H., 2019. High mountain areas. In: Pörtner, H.-O., Roberts, D.C., Masson-Delmotte, V., et al. (Eds.), IPCC Special Report on the Ocean and Cryosphere in a Changing Climate. https://www.ipcc.ch/srocc/chapter/chapter-2/.

Hu, Y., Fu, Q., 2007. Observed poleward expansion of the Hadley circulation since 1979. Atmos. Chem. Phys. 7, 5229–5236. https://doi.org/10.5194/acp-7-5229-2007.

Jansa, A., Homar, V., Romero, R., Alonso, S., Guijarro, J.A., Ramis, C., 2017. Extension of summer climatic conditions into spring in the Western Mediterranean area. Int. J. Climatol. 37, 1938–1950. https://doi.org/10.1002/joc.4824.

Kalnay, E., Kanamitsu, R., Kistler, W., Collins, D., Deaven, L., Gandin, M., Iredell, S., Saha, G., White, J., Woollen, Y., Zhu, M., Chelliah, W., Ebisuzaki, W., Higgins, J., Janowiak, K.C., Mo, C., Ropelewski, J., Wang, A., Leetmaa, R., Reynolds, R., Jenne, R., Jospeh, D., 1996. The NCEP/NCAR 40-year reanalysis project. Bull. Am. Meteor. Soc. 77, 437–472. https://doi.org/10.1175/1520-0477077<0437:TNYRP>2.0.CO;2.

Kendall, M.G., 1955. Rank Correlation Methods. Charles Griffin, London.

Klein, G., Vitasse, Y., Rixen, C., Marty, C., Rebetez, M., 2016. Shorter snow cover duration since 1970 in the Swiss Alps due to earlier snowmelt more than to later snow onset. Clim. Chang. 139, 637–649. https://doi.org/10.1007/s10584-016-1806-y.

Kuhn, M., 2014. Caret: Classification and Regression Training. R Package Version 6.0-30.

Lemus-Canovas, M., Lopez-Bustins, J.A., Martin-Vide, J., Royé, D., 2019. synoptReg: an R package for computing a synoptic climate classification and a spatial regionalization of environmental data. Environ. Modell. Soft. 118, 114–119. https://doi.org/10.1016/j.envsoft.2019.04.006.

Liaw, A., Wiener, M., 2012. Random forest: breiman and cutler's random forests for classification and regression. R Package Version 4.6-7.

López Moreno, J.I., Garcia Ruiz, J.M., 2004. Influence of snow accumulation and snowmelt on streamflow in the Central Spanish Pyrenees, International. J. Hydrol. Sci. 49, 787–802. https://doi.org/10.1623/hysj.49.5.787.55135.

López-Moreno, J.I., 2005. Recent variations of snowpack depth in the central Spanish Pyrenees. Arct. Antarct. Alp. Res. 37, 253–260. https://doi.org/10.1657/1523-0430(2005)037.

López-Moreno, J.I., Serrano-Vicente, S.M., 2006. Atmospheric circulation influence on the interannual variability of snowpack in the Spanish Pyrenees during the second half of the twentieth century. Nord. Hydrol. 38 (1), 38–44. https://doi.org/10.2166/nh.2007.030.

López-Moreno, J.I., Beguería, S., García-Ruiz, J.M., 2006. Trends in high flows in the Central Spanish Pyrenees: response to climatic factors or to land-use change? Hydrol. Sci. J. 51 (6), 1039–1050. https://doi.org/10.1623/hysj.51.6.1039.

Lopez-Moreno, J.I., García-Ruiz, J.M., Beniston, M., 2008. Environmental change and water management in the Pyrenees. Facts and future perspectives for Mediterranean mountains. Glob. Planet. Chang. 66, 300–312. https://doi.org/10.1016/j.gloplacha.2007.10.004.

López-Moreno, J.I., Goyette, S., Vicente-Serrano, S.M., Beniston, M., 2011. Effects of climate change on the intensity and frequency of heavy snowfall events in the Pyrenees. Clim. Chang. 105, 489–508. https://doi.org/10.1007/s10584-010-9889-3.

López-Moreno, J.I., Pomeroy, J.W., Revuelto, J., Vicente-Serrano, S.M., 2013. Response of snow processes to climate change: spatial variability in a small basin in the Spanish Pyrenees. Hydrol. Process. 27, 2637–2650. https://doi.org/10.1002/hyp.9408.

López-Moreno, J.I., Revuelto, J., Rico, I., Chueca-Cía, J., Julián, A., Serreta, A., Serrano, E., Vicente-Serrano, S.M., Azorin-Molina, C., Alonso-González, E., 2016. Thinning of the Monte Perdido glacier in the spanish pyrenees since 1981. Cryosph 10 (2), 681–694. https://doi.org/10.5194/tc-10-681-2016.

López-Moreno, J.I., Gascoin, S., Herrero, J., Sproles, E.A., Pons, M., Alonso-González, E., Hanich, L., Boudhar, A., Musselman, K.N., Molotch, N.P., Sickman, J., Pomeroy, J., 2017. Different sensitivities of snowpacks to warming in Mediterranean climate mountain areas. Environ. Res. Lett. 12 (7), 2017. https://doi.org/10.1088/1748-9326/aa70cb.

López-Moreno, J.I., Pomeroy, J.W., Alonso-González, E., Morán-Tejeda, E., Revuelto, J., 2020a. Decoupling of warming mountain snowpacks from hydrological regimes. Environ. Res. Lett. 15, 11–15. https://doi.org/10.1088/1748-9326/abb55f.

López-Moreno, J.I., Soubeyroux, J.M., Gascoin, S., Alonso-González, E., Durán-Gómez, N., Lafaysse, M., Vernay, M., Carmagnola, C., Morin, S., 2020b. Long-term trends (1958–2017) in snow cover duration and depth in the Pyrenees. Int. J. Climatol. 1-15 https://doi.org/10.1002/joc.6571.

Mann, H.B., 1955. Nonparametric tests against trend. Econometrica 13, 245–259.

Marcolini, G., Bellin, A., Disse, M., Chiogna, G., 2017. Variability in snow depth time series in the Adige catchment. J. Hydrol. Reg. Stud. 13, 240–254. https://doi.org/10.1016/j.ejrh.2017.08.007.

Marty, C., 2008. Regime shift of snow days in Switzerland. Geophys. Res. Lett. 35, L12501.

Matiu, M., Crespi, A., Bertoldi, G., Carmagnola, C.M., Marty, C., Morin, S., Schöner, W., Cat Berro, D., Chiogna, G., De Gregorio, L., Kotlarski, S., Majone, B., Resch, G., Terzago, S., Valt, M., Beozzo, W., Cianfarra, P., Gouttevin, I., Marcolini, G., Notarnicola, C., Petitta, M., Scherrer, S.C., Strasser, U., Winkler, M., Zebisch, M., Cicogna, A., Cremonini, R., Debernardi, A., Faletto, M., Gaddo, M., Giovannini, L., Mercalli, L., Soubeyroux, J.-M., Susnik, A., Trenti, A., Urbani, S., Weilguni, V., 2020. Observed snow depth trends in the European Alps 1971 to 2019. Cryoph 2020, 1–50. https://doi.org/10.5194/tc-2020-289.

Morán-Tejeda, E., Lorenzo-Lacruz, J., López-Moreno, J.I., Rahman, K., Beniston, M., 2014. Streamflow timing of mountain rivers in Spain: recent changes and future projections. J. Hydrol. 517, 1114–1127. https://doi.org/10.1016/j.jhydrol.2014.06.053.

Musselman, K.N., Clark, M.P., Liu, C., Ikeda, K., Rasmussen, R., 2017. Slower snowmelt in a warmer world. Nat. Clim. Chang. 7 (3), 214–219. https://doi.org/10.1038/nclimate3225.

Navarro-Serrano, F., López-Moreno, J.I., 2017. Spatio-temporal analysis of snowfall events in the Spanish Pyrenees and their relationship to atmospheric circulation. Cuad. Invest. Geogr. 43 (1), 233–254. https://doi.org/10.18172/cig.3042.

Nogués-Bravo, D., Lasanta, T., López-Moreno, J.I., Araújo, M.B., 2008. Climate warming in Mediterranean mountains during the XXIst century. Ambio 37 (4), 280–285. https://doi.org/10.1579/0044-7447(2008)37.

Oliva, M., Ruiz-Fernández, J., Barriendos, M., Benito, G., Cuadrat, J.M., García-Ruiz, J. M., Giralt, S., Gómez- Ortiz, A., Hernández, A., López-Costas, O., López-Moreno, J.I., López-Sáez, J.A., Martínez- Cortizas, A., Moreno, A., Prohom, M., Saz, M.A., Serrano, E., Tejedor, E., Trigo, R., Valero-Garcés, B.L., Vicente- Serrano, S., 2018. The Little Ice Age in Iberian mountains. Earth Sci. Rev. 177, 175–188. https://doi.org/10.1016/j.earscirev.2017.11.010.

OPCC-CTP, 2018. Climate Change in the Pyrenees: Impacts, Vulnerabilities and Adaptation Bases of Knowledge for the Future Climate Change Adaptation Strategy in the Pyrenees, 147 pp, Jaca, Spain. https://www.opccctp.org/sites/default/files/editor/opcc-informe-en-paginas.pdf (last access: 21 November 2021).

Pagès, M., Pepin, N., Miró, J.R., 2017. Measurement and modelling of temperature cold pools in the Cerdanya valley (Pyrenees), Spain. Met. Apps. 24, 290–302. https://doi.org/10.1002/met.1630.

Patakamuri, S.K., O'Brien, N., Patakamuri, M.S.K., 2017. Package "Modifiedmk".

Philipp, A., Beck, C., Huth, R., Jacobeit, J., 2014. Development and comparison of circulation type classifications using the COST 733 dataset and software. Int. J. Climatol. 36, 2673–2691. https://doi.org/10.1002/joc.3920.

Pons, M., López-Moreno, J.I., Rosas-Casals, M., Jover, È., 2015. The vulnerability of Pyrenean ski resorts to climate-induced changes in the snowpack. Clim. Chang. 131, 591–605. https://doi.org/10.1007/s10584-015-1400-8.

R Core Team, 2018. R: A Language and Environment for Statistical Computing. R Foundation for Statistical Computing, Vienna. https://www.R-project.org/.

Rebetez, M., Reinhard, M., 2008. Monthly air temperature trends in Switzerland 1901-2000 and 1975-2004. Theor. App. Climatol. 91, 27–34. https://doi.org/10.1007/s00704-007-0296-2.

Reid, P.C., Hari, R.E., Beaugrand, G., Livingstone, D.M., Marty, C., Straile, D., Barichivich, J., Goberville, E., Adrian, R., Aono, Y., Brown, R., Foster, J., Groisman, P., Hélaouët, P., Hsu, H.H., Kirby, R., Knight, J., Kraberg, A., Li, J., Lo, T.T., Myneni, R.B., North, R.P., Pounds, J.A., Sparks, T., Stübi, R., Tian, Y., Wiltshire, K.H., Xiao, D., Zhu, Z., 2016. Global impacts of the 1980s regime shift. Glob. Chang. Biol. 22, 682–703. https://doi.org/10.1111/gcb.13106.

Renard, B., Lang, M., Bois, P., Dupeyrat, A., Mestre, O., Niel, H., Sauquet, E., Prudhomme, C., Parey, S., Paquet, E., Neppel, L., Gailhard, J., 2008. Regional methods for trend detection: assessing field significance and regional consistency. Water Resour. Res. 44 (8) https://doi.org/10.1029/2007WR006268.

Rico, I., Izagirre, E., Serrano, E., López-Moreno, J.I., 2017. Superficie glaciar actual en los Pirineos: Una actualización para 2016. Pirineos 172, 29. https://doi.org/10.3989/Pirineos.2017.172004.

Saffioti, C., Fischer, E.M., Scherrer, S.C., Knutti, R., 2016. Reconciling observed and modeled temperature and precipitation trends over Europe by adjusting for circulation variability. Geophys. Res. Lett. 43, 8189–8198. https://doi.org/10.1002/2016GL069802.

Sanchez-Lorenzo, A., Calbó, J., Wild, M., 2013. Global and diffuse solar radiation in Spain: building a homogeneous dataset and assessing their trends. Glob. Planet. Chang. 100, 343–352. https://doi.org/10.1016/J.GLOPLACHA.2012.11.010.

Sanchez-Lorenzo, A., Enriquez-Alonso, A., Wild, M., Trentmann, J., Vicente-Serrano, S.M., Sanchez-Romero, A., Hakuba, M., 2017. Trends in downward surface solar radiation from satellites and ground observations over Europe during 1983–2010. Remote Sens. Environ. 189, 108–117. https://doi.org/10.1016/j.rse.2016.11.018.

Scherrer, S.C., Appenzeller, C., 2006. Swiss Alpine snow pack variability: major patterns and links to local climate and large-scale flow. Clim. Res. 32, 187–199. https://doi.org/10.3354/cr032187.

Schöner, W., Koch, R., Matulla, C., Marty, C., Tilg, A.M., 2018. Spatiotemporal patterns of snow depth within the Swiss Austrian Alps for the past half century (1961 to 2012) and linkages to climate change. Int. J. Climatol. 39 (3), 1589–1603. https://doi.org/10.1002/joc.5902.

Schwartz, A., McGowan, H., Theobald, A., Callow, N., 2020. Quantifying the impact of synoptic weather types, patterns, and trends on energy fluxes of a marginal snowpack. Cryosph. 14, 2755–2774. https://doi.org/10.5194/tc-14- 2755-2020.

Seidel, D.J., Randel, R.J., 2007. Recent widening of the tropical belt: evidence from tropopause observations. J. Geophys. Res. 112, D20113. https://doi.org/10.1029/2007JD008861.

Sen, P.K., 1968. Estimates of the regression coefficient based on Kendall's Tau. J. Am. Stat. Assoc. 63 (324), 1379. https://doi.org/10.2307/2285891.

Sippel, S., Fischer, E.M., Scherrer, S.C., Meinshausen, N., Knutti, R., 2020. Late 1980s abrupt cold season temperature change in Europe consistent with circulation variability and long-term warming. Environ. Res. Lett. 15, 094056 https://doi.org/10.1088/1748-9326/ab86f2.

Suriano, Z.J., Leathers, D.J., 2018. Great lakes basin snow-cover ablation and synoptic-scale circulation. J. Appl. Meteorol. Climatol. 57, 1497–1510. https://doi.org/10.1175/JAMC-D-17-0297.

Valt, M., Cianfarra, P., 2010. Recent snow cover variability in the Italian alps. Cold Regions Sci. Tech. 64 (2), 146–157. https://doi.org/10.1016/j.coldregions.2010.08.008.

Vernay, M., Lafaysse, M., Monteiro, D., Hagenmuller, P., Nheili, R., Samacoïts, R., Verfaillie, D., Morin, S., 2021. The S2M meteorological and snow cover reanalysis over the French mountainous areas, description and evaluation (1958–2020). Earth Syst. Sci. Data Discuss. https://doi.org/10.5194/essd-2021-249.

Vicente-Serrano, S.M., Rodríguez-Camino, E., Domínguez-Castro, F., El Kenawy, A., Azorín-Molina, C., 2017. An updated review on recent trends in observational Surface atmospheric variables and their extremes over Spain. Cuad. Inv. Geogr. 43, 209. https://doi.org/10.18172/cig.3134.

Vidaller, I., Revuelto, J., Izagirre, E., Rojas-Heredia, F., Alonso-González, E., Gascoin, S., René, P., Berthier, E., Rico, I., Moreno, A., Serrano, E., Serreta, A., López-Moreno, J.I., 2021. Toward an ice-free mountain range: Demise of Pyrenean glaciers during 2011–2020. J. Geophys. Res. Lett. 48, e2021GL094339 https://doi.org/10.1029/2021GL094339.

Vilar-Bonet, F., Salvador-Franch, F., 1996. Variaciones y tendencia secular de la precipitación de nieve en Andorra (Pirineo Oriental). In: Marzol, M., Dorta, P., Valladares, P. (Eds.), Clima y agua: la gestión de un recurso climático, pp. 87–97. La Laguna.

Vionnet, V., Brun, E., Morin, S., Boone, A., Faroux, S., Le Moigne, P., Martin, E., Willemet, J.M., 2012. The detailed snowpack scheme Crocus and its implementation in SURFEX v7.2. Geosci. Model Dev. 5, 773–791. https://doi.org/10.5194/gmd-5-773-2012.

Vorkauf, M., Marty, C., Kahmen, A., Hiltbrunner, E., 2021. Past and future snowmelt trends in the Swiss Alps: the role of temperature and snowpack. Clim. Chang. 165, 3–4. https://doi.org/10.1007/s10584-021-03027-x.

Wild, M., 2009. Global dimming and brightening: A review. J. Geophys. Res. 114, D00D16. https://doi.org/10.1029/2008JD011470.

Yasunaka, S., Hanawa, K., 2002. Regime shifts found in the Northern Hemisphere SST field. J. Meteorol. Soc. Jpn. 80, 119–135. https://doi.org/10.2151/jmsj.80.119.